Automatic Data-Driven Parameterization for Phase-Based Bone Localization in US Using Log-Gabor Filters

Ilker Hacihaliloglu[1], Rafeef Abugharbieh[1], Antony Hodgson[2], and Robert Rohling[1,2]

[1] Department of Electrical and Computer Engineering
[2] Department of Mechanical Engineering, University of British Columbia, Vancouver, BC, Canada
ilkerh@ece.ubc.ca, rafeef@ece.ubc.ca, ahodgson@mech.ubc.ca, rohling@ece.ubc.ca

Abstract. Intensity-invariant local phase-based feature extraction techniques have been previously proposed for both soft tissue and bone surface localization in ultrasound. A key challenge with such techniques is optimizing the selection of appropriate filter parameters whose values are typically chosen empirically and kept fixed for a given image. In this paper we present a novel method for contextual parameter selection that is adaptive to image content. Our technique automatically selects the scale, bandwidth and orientation parameters of Log-Gabor filters for optimizing the local phase symmetry in ultrasound images. The proposed approach incorporates principle curvature computed from the Hessian matrix and directional filter banks in a phase scale-space framework. Evaluations performed on in vivo and in vitro data demonstrate the improvement in accuracy of bone surface localization compared to empirically set parameterization results.

Keywords: Ultrasound, local phase features, principle curvature, automatic parameter selection, phase symmetry, bone localization, Log Gabor filters.

1 Introduction

Extraction of tissue and bone boundaries from ultrasound (US) images is particularly challenging due to the typically low signal-to-noise ratio and the presence of artifacts which significantly complicate image interpretation and automatic processing. Image intensity and gradient based methods have shown some promise but still remain highly influenced by the image intensity variations and imaging artifacts [1,2]. Intensity invariant local phase based feature extraction has attracted some attention and has been shown to be very promising for processing US images of soft tissue [3] and, more recently, bone surfaces [4].

Although local phase measures can be quite successful in extracting important image features, they remain somewhat sensitive to the underlying filter parameters used. Previous approaches using local phase relied on empirical selection of appropriate filter parameters, which was typically performed by trial and error and ad hoc investigation of filter outputs on samples of US images depicting a certain anatomical area

G. Bebis et al. (Eds.): ISVC 2009, Part I, LNCS 5875, pp. 944–954, 2009.

of interest [3-5]. Once acceptable filter parameters are found, they are typically fixed for subsequent application to new data. The difficulty in relating correct parameter choices to the properties of the image and image-processing task has inhibited more widespread use of phase-based techniques.

In this work, we present a novel method for automatically selecting the scale, bandwidth, orientation and angular bandwidth parameters of the Log-Gabor filter for calculating phase symmetry (PS) measures in US images, specifically in the context of bone surface localization. The proposed approach incorporates the use of principal curvature computed from the Hessian matrix and directional filter banks in a phase scale-space framework. To the best of our knowledge, this is the first study that investigates the automatic selection of these different parameters for ultrasound images. Our technique relies on contextual information obtained solely from the image content. Qualitative and quantitative evaluations performed on *in vivo* and *in vitro* scans demonstrate the utility of the our parameter selection approach, its insensitivity to artifacts when detecting bone boundaries, and the improvements achieved in terms of surface localization accuracy.

2 Methods

We address the problem of filter parameter selection within the context of localization of bone surfaces in US images, which is one of the emerging imaging modalities in computer assisted orthopaedic surgery (CAOS) applications [1,2,4,5]. Hacihaliloglu *et al* recently presented a local phase-based method for extracting ridge-like features similar to those that occur at soft tissue/bone interfaces using a PS measure [4]. We propose an improvement to such an approach by proposing a complete automation of the parameter selection process. The current paper focuses on extraction of ridge-like features but could be extended to other feature types.

Local phase information is computed by convolving the image with a quadrature pair of band pass filters. In this work, we use the Log-Gabor filter [3-5]. This orientation-dependent 2D Log-Gabor filter is defined in the frequency domain (ω) by multiplying a one dimensional Log Gabor function that controls the frequencies to which the filter responds with an angular Gaussian function that controls the orientation selectivity of the filter (1):

$$G(\omega,\phi) = \exp\left(\frac{(\log(\omega/\omega_0))^2}{2(\log(\kappa/\omega_0))}\right)\times\exp\left(\frac{(\phi-\phi_0)^2}{2\sigma_\phi}\right) \quad (1)$$

where κ is the standard deviation of the filter in the radial direction and ω_0 is the filter's center spatial frequency. The term κ/ω_0 is related to the bandwidth (β) of the filter with $\beta = -2\,(2/\ln 2)^{(-0.5)}\ln(\kappa/\omega_0)$. The scaling of the radial Log Gabor function is achieved by using different wavelengths which are based on multiples of a minimum wavelength, λ_{min}. Angular bandwidth σ_ϕ is the standard deviation of the Gaussian spreading function in the angular direction that describes the filter's angular selectivity. To obtain higher orientation selectivity, the angular function must become narrower. Steering of the filter is achieved by changing its angle (ϕ_0). In the following sections, we analyze the Log-Gabor filter response in detail and present a data-driven approach for contextual selection of the main filter parameters: bandwidth, orientation, scale and angular

bandwidth. We first demonstrate how to select the optimal filter bandwidth based on image acquisition parameters, and then proceed to select the filter orientations, scale and angular bandwidth.

2.1 Filter Bandwidth Selection

The proper filter bandwidth (β= -2 $(2/\ln 2)^{(-0.5)}\ln(\kappa/\omega_0)$) in the radial direction is related to both the spatial extents of the speckle and boundary responses in the image. Therefore, we first estimate the image speckle size by selecting a set of images covering a range of depths and acquired by the same US transducer (center ultrasound frequency = 7.5 MHz, image sizes ranged between 1.9cm-7.2cm), isolating a region with fully developed speckle from each image, computing the autocorrelation of each region, and extracting the full-width at half-maximum (FWHM) of these autocorrelations as a measure of the speckle size [6]. We compute the ratio, κ/ω_0, for each image using (2):

$$\kappa / \omega_0 = \exp(-\frac{1}{4}\sqrt{2 \times ln(2)} \times FWHM \times r) \tag{2}$$

where r is the pixel size in mm, and average the κ/ω_0 ratio over the set of 25 different B-mode US test images; the resulting average is chosen as the filter bandwidth. Selecting a bandwidth significantly greater than this (ie, selecting a smaller value for κ/ω_0) will result in a filter that fails to separate small scale speckle features from larger scale boundary responses. Selecting a significantly lower bandwidth will reduce the accuracy of the boundary detection and cause blurring of the detected bone boundary (Fig.1).

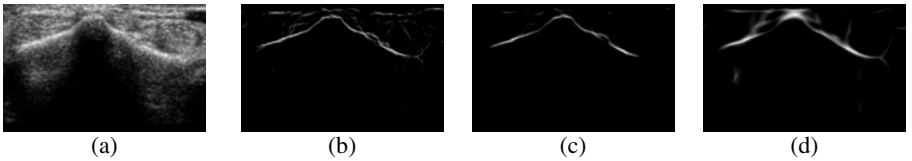

Fig. 1. Effect of filter bandwidth on local phase based bone detection. (a) *in vivo* B-mode US image of human distal radius, (b) – (d) PS images obtained using κ/ω_0 values of 0.05, 0.24, and 0.55 respectively. (b) illustrates unintended speckle detection at high bandwidths and (d) illustrates bone boundary blurring at low bandwidths.

2.2 Filter Scale Selection

Local image PS is computed by convolving the image with a number of scaled Log-Gabor filters. Each scaling is designed to pick out particular features of the image being analyzed with results typically integrated over multiple scales (in addition to multiple orientations) [4]. Since boundaries are extracted by analyzing the PS measure over a range of scales, correct scale selection is of major importance.

When using very small scales, the filters become highly sensitive to speckle. Selecting larger scales blurs the extracted bone features. Simply integrating different filter scales for PS calculations is insufficient resulting in PS images that extract speckle or blurring the detected features (in our case bone boundaries), as demonstrated in Fig. 2.

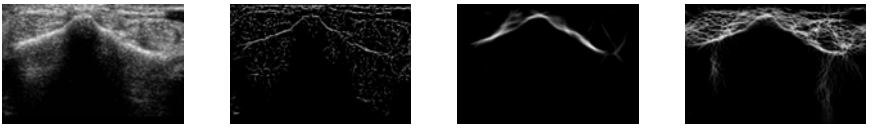

Fig. 2. Effects of filter scale selection. (a) Original B-mode US image of *in vivo* distal radius, (b) PS obtained using a scale value of λ_{min} =2, (c) PS obtained using a scale value of λ_{min} =88, (d) PS obtained by combining the results of both scales (2 and 88).

Line enhancing filters based on multiscale eigenvalue analysis of the Hessian matrix have been commonly used to extract vessel-like structures in 2D and 3D medical images [7]. The scale selection approach we present in this paper is inspired by these studies where we use the Log-Gabor filter response as the input to the Hessian matrix defined as in (2):

$$H = \begin{bmatrix} L_{xx} & L_{xy} \\ L_{yx} & L_{yy} \end{bmatrix}, \text{with } L_{ab} = \frac{\partial^2 L}{\partial a \partial b} \tag{2}$$

L is an image obtained convolving the US image with a Log-Gabor filter at a particular scale. Here, the subscripts *x* and y represent spatial derivatives in the *x* and *y* directions. At this stage, the orientation of the Log-Gabor filter during the scale setting step is set to the initial filter angle calculated from the B-mode US image as explained below in the filter orientation selection step We calculate a ridge strength measure as $A_\gamma = t^{2\gamma}((L_{xx}-L_{yy})^2+4L_{xy}^2)$, which is the square of the γ normalized eigenvalue difference, and *t* is the scale of the filter ($t = \lambda_{min}$) [8]; see Fig. 3. This metric in our context measures the 'ridgeness content' of an image, since our main interest here is in localizing bone contours, which generally appear as ridges in US images. The optimal scale is then defined as the one corresponding to the maximal ridgeness content in the Gabor filtered image. In order to define the optimum global filter scale, which gives

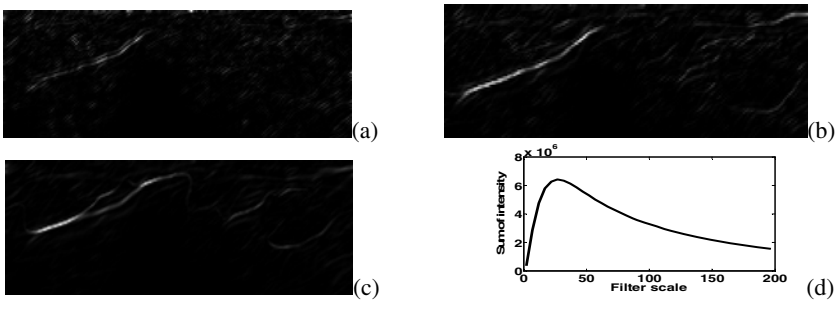

Fig. 3. Effects of filter bandwidth selection. A_γ ridge strength obtained from B-mode US image in Fig.1 (a) for a fixed filter orientation (140°) and scale (a) λ_{min}=10, (b) λ_{min}=35, (c) λ_{min}=140. Investigating (a)-(c) we see that the bone ridge content in (b) is the strongest and the most continuous. (d) Filter scale versus sum of intensity values of A_γ.

the most significant ridge content in the image, we analyze the intensity distribution of A_γ over all possible scales (e.g. ranging from 2-150) and select the scale where the sum of the intensities reaches a maximum value as our optimal filter scale (Fig.3 (d)). This is based on the observation that at the optimal scale the response of the filter will produce a sharp ridge feature aligned with the bone surface, whereas significantly different scales will result either in detection of speckle or blurred bone surfaces which will give a smaller intensity sum (Fig. 3 (a)–(c)). This analysis is repeated for each orientation separately.

2.3 Filter Orientation Selection

The orientation of the Log Gabor filter is controlled by the angular Gaussian function used in (1). During the calculation of the PS metric, the filter is directed at a number of orientations. Commonly, six orientations are employed to cover the entire angular range (0°-180° with 30° increments) with the responses subsequently averaged [3-5].

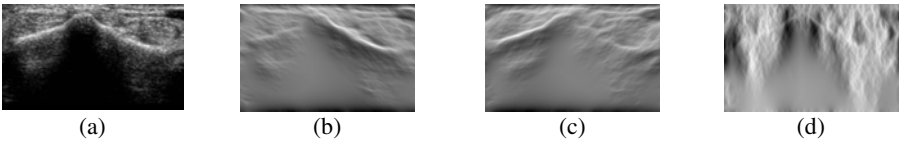

(a) (b) (c) (d)

Fig. 4. Effects of filter orientation selection. (a) B-mode US of *in vivo* distal radius, (b) filter response at ϕ=60°, (c) filter response at ϕ=120°, (d) filter response at ϕ=0°. All images were produced at a fixed filter scale of λ_{min} =25 and κ/ω_0=0.25.

However, given the highly directional nature of ultrasound bone image data, integration of the responses at all of these different filter orientations in fact largely degrades the PS response due to the inclusion of many non-relevant filter orientations. Noting that the strongest ridge features appear when the filter orientation is perpendicular to the bone surface (Fig. 4), identifying and combining filter angles which produce strong responses will therefore likely enhance feature extraction (Fig. 5).

Bone surfaces in US images typically appear as elongated line-like objects with a higher intensity compared to the other features. The same analysis is true for the PS images. Therefore, integration along a bony feature produces a higher intensity value than doing the integration along a non-bony feature. We thus make use of a simple radon transform (RT) in order to detect the orientation of such line-like structures. In order to automatically define meaningful starting angles for our filter, we initially cluster the RT (obtained from the B-mode US image) image using k-means clustering (Fig. 6).

The projection angles corresponding to the peak values of the RT reflect the angles that are perpendicular to the high intensity features, such as bone surfaces. Those angles are therefore used for initializing the orientations of the Log-Gabor filter. In order to obtain three initial filter angles, we chose the cluster that corresponds to the peak values of the RT (Fig. 6. (c)) and calculated the mean value of the projection angles corresponding to the RT values in that chosen cluster. This calculated mean value is used as the initial angle, and we add two additional angles set at ±1 standard deviation within the thresholded region. These three initial angles are used as the filter angles during the calculation of the filter scale as explained in section 2.2.

Fig. 5. Effect of varying the number of orientations used. (a) B-mode US image of *in vivo* human distal radius. (b) PS image using 3 orientations (58° 74° 89°), (b) PS image using 6 orientations (0°-150° with 30° increments), (c) PS image using 10 orientations (0°-270° with 30° increments). White arrows point out the extracted phase features which are not bone surfaces obtained by combining orientations which are not perpendicular to the bone surface during the calculation of PS. The white circle points to a location of a degraded bone surface due to the inclusion of less informative orientations with weaker bone responses.

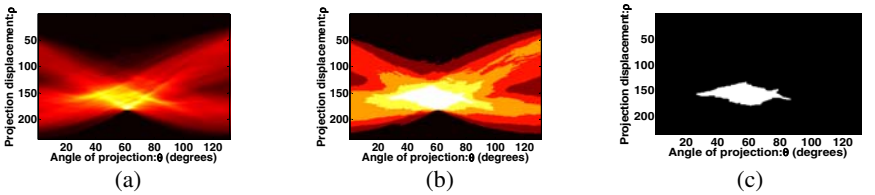

Fig. 6. Filter orientation selection. (a) RT of B-mode US image in Fig.1 (a), (b) clustered RT of (a), (c) the cluster corresponding to the highest RT values. The three initial angles deduced from this cluster are 66°, 88° and 106° (refer to text for details about the calculation of these three angles).

In order to obtain the final filter orientations, the RT is re-calculated for the ridge strength image A_γ as obtained using the scale calculated in section 2.2. Figure 7 shows the calculated RT of the A_γ for the initial angles of 66° and 106°. Investigating the figures, we note that the RT has high intensity locations indicating the presence of line-like structures in the image. The maximum value of the RT indicates the main orientation of the bone, since it has the strongest filter response, and is thus used to set the filter orientation. Figure 7 (c) and (d) show an example where the angles corresponding to the peak occur at 62° and 115°, hence the initial angles will be corrected based on these new calculated angles.

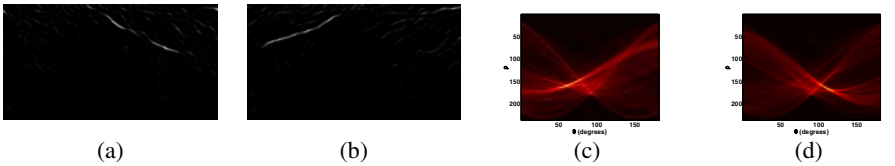

Fig. 7. Filter orientation selection. (a) & (b): A_γ obtained using the initial filter angle ϕ=66° (a) and ϕ=106° (b) which are calculated from the RT of the B-mode image, (c) & (d) RT of (a) & (b) showing new peaks at 62° and 115°, respectively.

2.4 Filter Angular Bandwidth Selection

The angular bandwidth σ_{ϕ} parameter corresponds to the standard deviation of the Gaussian spreading function in the angular direction and describes the filter's angular selectivity. Investigating the example in Fig. 7, we can see that at large angular bandwidths the Log-Gabor filter acts as a smoothing filter without being sensitive to any orientation. On the other hand, for small angular bandwidths, the filter acts like a line detector degrading the curvature of the bone surface as it becomes less sensitive to curvature making the extracted features look like short line segments. Therefore, using the same analysis we used in our filter scale selection process would not be suitable to set σ_{ϕ} since the intensity distribution of A_{γ} over all possible angular bandwidths will give a peak for very large angular bandwidths (Fig. 9 (a)) which would correspond to a filter response shown in Fig.8 (a).

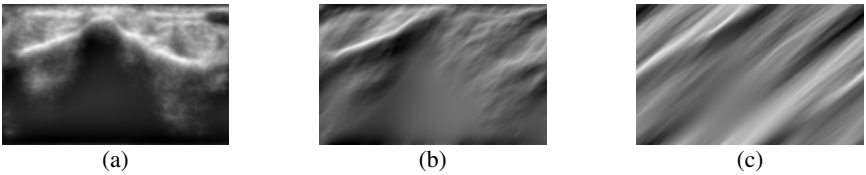

(a) (b) (c)

Fig. 8. Effect of varying angular bandwidth on the Log-Gabor filter output for filter orientation 115°. (a) σ_{ϕ}=120°, (b) σ_{ϕ} =30°, (c) σ_{ϕ} =7.5°.

Based on the above observations, we analyze the kurtosis of the RT of A_{γ} over different angular bandwidth values. We select the bandwidth corresponding to the peak kurtosis value (Fig.8 (b)). During this stage, the A_{γ} images used are obtained using the optimum filter scale as calculated in section 2.2.

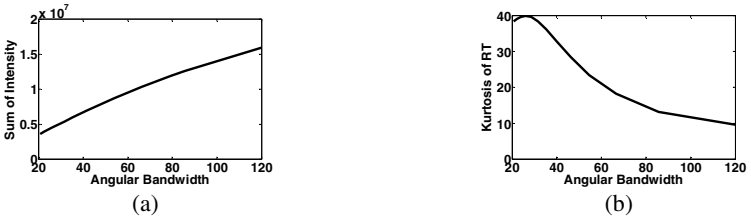

(a) (b)

Fig. 9. Angular bandwidth selection. (a) Filter angular bandwidth versus sum of intensity values of A_{γ}. (b) filter angular bandwidth versus kurtosis of RT obtained from calculating the RT of A_{γ}.

2.5 Experimental Setup for Quantitative Validation

We constructed a phantom comprised of an *ex vivo* bovine femur specimen inside an open-topped plexiglass cylindrical tube (Fig. 10). Twenty-eight markers (1mm diameter steel balls) were added to the construct with fourteen beads placed on each side of the bone (longitudinally) and spaced at equal axial intervals over a distance of 75 mm. We obtained US scans of this specimen where the volumes containing 16 fiducials (8

on each side) spanning a region of 37.8mm. To hold the specimen and fiducials in place during the scanning procedures, the tube was filled with a firm gel (Super Soft Plastic, M-F Manufacturing, Texas, USA). We note that we did compensate for the difference in the speed of sound in soft tissue and gel during the image reconstruction process.

The constructed phantom was scanned in an Xtreme CT machine with isometric 0.25 mm voxels. US scanning was performed using a 3D GE Voluson 730 Expert system (GE Healthcare, Waukesha, WI) with a 3D RSP5-12 probe. The US data was subsequently rescaled to match the resolution of the CT image. Also, a fiducial-based rigid-body registration was applied to align the CT and US volumes. Following registration, bone surfaces were extracted from CT scan using a simple thresholding operation to establish a gold standard bone surface. Bone surfaces were then extracted from the US data using the discussed PS features, both with and without the parameters optimized.

(a) (b)

Fig. 10. Quantitative validation experiment. (a) Picture of the constructed phantom, (b) Axial view schematic sketch of the phantom.

The accuracy of bone localization in US (PS filtered scans) was quantitatively assessed by averaging the PS response at voxels corresponding to varying distances from the real bone surface (as obtained from the CT gold standard). To achieve this, we studied a set of (intensity, distance) pairs using the signed distance transform. High intensity values confined to a zone near zero distance would indicate an accurately located surface. Our surface matching error was hence defined by the average signed distance values corresponding to the maximum phase intensity value along each vertical column of the 2D PS images.

3 Results

Implementation Details: The proposed method was implemented in MATLAB (The Mathworks Inc., Natick, MA, USA). The filter bandwidth was calculated as 0.24 by using the proposed method in section 2.1. During the scale selection process the γ value was set to 0.75 since this was reported to be optimal value for ridge feature detection [8]. For filter orientation we chose to work with three angles since choosing greater than three orientations had an insignificant effect on the results.

Quantitative Results: The surface matching mean error was 0.64 mm (std 1.34) with the best empirically-set parameters compared to 0.51mm (std 0.64) for our proposed automatically-set parameters. Choosing two scales for the empirical method decreases

the surface matching mean error to 0.54mm (std: 1.82) but introduces more outlier points away from the zero signed distance indicating an increase in the detection of US artifacts.

Qualitative Results: Figure 11 shows a qualitative comparison of PS images of a *in vivo* human distal radius and pelvis obtained with the proposed optimized Gabor filter paramters and contrasted to the best values that could be empirically set. Note how the local phase images obtained empirically using 2 scales extracted more US artifacts and resulted in a thicker bone boundary due the unsuitable scale combination. Moreover, integrating the zero angle as one of the filter orientations caused the detection of unwanted features on the sides of the bone surface (Fig. 6.white arrows). Decreasing the filter scale to 1 in the empirical case caused gaps in the extracted bone surfaces (Fig. 6.white circles). Our surface results on the other hand, which used optimized filter parameters, were consistently sharper with reduced unwanted features on the

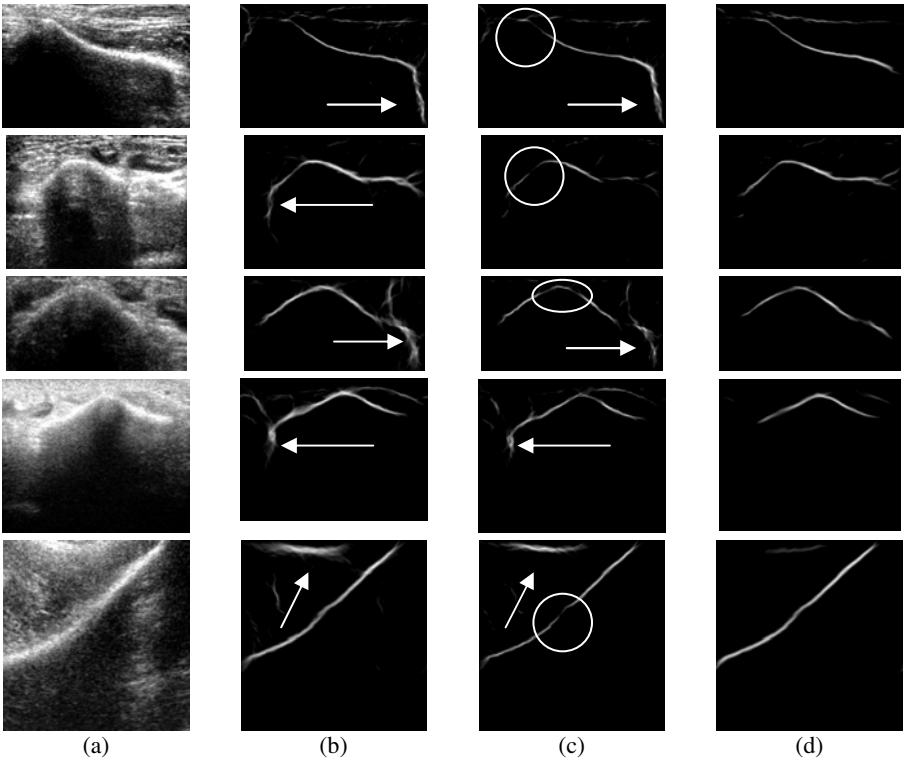

Fig. 11. Qualitative results. (a) B-mode US image of in vivo distal radius (rows1-4) and pelvis (row 5) areas. Imaging depth of the US machine was 3.5, 3.5, 1.9, 4.5 and 4.9cm, respectively. (b) Non-optimized PS images using two different filter scales (25 and 75), (c) Non-optimized PS images using one scale only (25)(d) PS images obtained using the proposed optimized parameters. White arrows point out the extracted phase features which are not bone surfaces obtained by combining orientations which are not perpendicular to the bone surface during the calculation of PS. The white circles points to a location of a degraded bone surface due to the inclusion of less informative orientations with weaker bone responses.

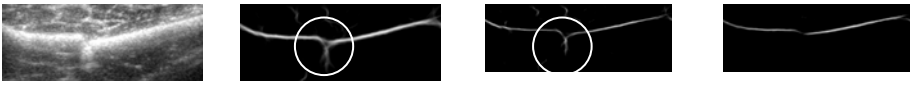

Fig. 12. Qualitative results on fractured *ex vivo* porcine tibia fibula specimen. (a) B-mode US image, (b) Non-optimized PS images using two filter scales (25 and 75), (c) Non-optimized PS images using one scale only (25), (d) PS images obtained using the proposed optimized parameters. The white circles point out the extracted phase features which are not bone surfaces obtained by combining orientations which are not perpendicular to the bone surface during the calculation of PS.

bone sides and with no gaps in the detected surfaces. Figure 12 shows other qualitative examples where scans of a fractured *ex-vivo* porcine tibia fibula specimen were acquired. Note how the proposed method produced a cleaner identification of the bone fracture.

4 Discussion and Conclusions

Though local image phase information has been successfully applied for extracting US image features, none of the prior studies has investigated the effects of parameter selection on the extracted features nor provided guidelines on how this could be achieved. In this paper, we proposed a novel approach for automatic selection of the scale, bandwidth and orientation of Log-Gabor filters for calculating phase symmetry responses in bone US. For scale selection, we used a ridgeness content measure obtained from the Hessian matrix eigenvalues to investigate the information content extracted at different scales. For orientation selection, the appearance of bone surfaces was incorporated within our framework where the RT obtained from the image ridgeness content measure was used to deduce the optimal angles of the directional filter. We analyzed US images with fully developed speckle and measured the image speckle size by calculating the autocorrelation function to determine the filter bandwidth. Finally the angular bandwidth was calculated by investigating the kurtosis of the RT obtained from the image ridgness content measure. We presented qualitative results obtained from *in vivo* and *ex vivo* scans and demonstrated the critical importance of selecting the correct scales and orientations in local phase based US processing. Quantitative results were also presented on a specially constructed bone phantom where the gold standard surface of the bone was established through CT imaging. An improvement of close to 0.2mm in bone localization accuracy was observed. Future work will include the extension of this automatic parameter selection method to 3D and a clinical study where the proposed method will be tested on scans obtained from patients with distal radius and pelvis fractures.

References

1. Barratt, D.C., Penney, P.G., Chan, S.K., Slomczykowski, M., Carter, T.J., Edwards, P.J., Hawkes, D.J.: Self calibrating 3D-ultrasound-based bone registration for minimally invasive orthopaedic surgery. IEEE Transactions on Medical Imaging 25, 312–323 (2006)

2. Kowal, J., Amstutz, C., Langlotz, F., Talib, H., Ballester, M.: Automated bone contour detection in ultrasound B-mode images for minimally invasive registration in computer assisted surgery an *in vitro* evaluation. The International Journal of Medical Robotics and Computer Assisted Surgery, 341–348 (2007)
3. Mulet-Parada, M., Noble, J.A.: 2D+T boundary detection in echocardiography. Medical Image Analysis 4(1), 21–30 (2000)
4. Hacihaliloglu, I., Abugharbieh, R., Hodgson, A.J., Rohling, R.: Bone segmentation and fracture detection in ultrasound using 3D local phase features. In: Metaxas, D., Axel, L., Fichtinger, G., Székely, G. (eds.) MICCAI 2008, Part I. LNCS, vol. 5241, pp. 287–295. Springer, Heidelberg (2008)
5. Hacihaliloglu, I., Abugharbieh, R., Hodgson, A.J., Rohling, R.N.: Enhancement of bone surface visualization from 3D ultrasound based on local phase information. In: Proc. IEEE Ultrasonics Symposium, pp. 21–24 (2006)
6. Wagner, R.F., Smith, S.W., Sandrik, J.M., Lopez, H.: Statistics of Speckle in Ultrasound B-Scans. IEEE Transactions on Sonics and Ultrasonics, 156–163 (1983)
7. Frangi, A., Niessen, W., Vincken, K., Viergever, M.: Multiscale vessel enhancement filtering. In: Wells, W.M., Colchester, A.C.F., Delp, S.L. (eds.) MICCAI 1998. LNCS, vol. 1496, pp. 130–137. Springer, Heidelberg (1998)
8. Lindeberg, T.: Edge detection and ridge detection with automatic scale selection. International Journal of Computer Vision 30, 117–154 (1998)
9. Coifman, R.R., Wickerhouser, M.V.: Entropy based algorithms for best basis selection. IEEE Transaction on Information Theory (1992)